ENGINEERING

Structural tuning of heterogeneous molecular catalysts for electrochemical energy conversion

Jiong Wang[1,2,3], Shuo Dou[3], Xin Wang[3]*

Heterogeneous molecular catalysts based on transition metal complexes have received increasing attention for their potential application in electrochemical energy conversion. The structural tuning of first and second coordination spheres of complexes provides versatile strategies for optimizing the activities of heterogeneous molecular catalysts and appropriate model systems for investigating the mechanism of structural variations on the activity. In this review, we first discuss the variation of first spheres by tuning ligated atoms; afterward, the structural tuning of second spheres by appending adjacent metal centers, pendant groups, electron withdrawing/donating, and conjugating moieties on the ligands is elaborated. Overall, these structural tuning resulted in different impacts on the geometric and electronic configurations of complexes, and the improved activity is achieved through tuning the stability of chemisorbed reactants and the redox behaviors of immobilized complexes.

INTRODUCTION

Electrochemical energy conversion represents a promising approach to alleviate our dependence on fossil fuels, as it allows the utilization of renewable energy sources, which are subject to intermittence and geographic dependence, and stores in the form of chemical fuels (*1*–*4*). In recent years, various electrochemical conversion processes, such as H_2O splitting and CO_2 reduction, have been intensively studied, in which the key barrier lies in the development of efficient and low-cost catalysts (*5*–*10*). Among various types of catalysts, heterogeneous molecular catalysts, which are commonly obtained from immobilizing free-standing transition metal (TM) complexes onto solid supports (*11*, *12*), exhibit great potential. The active sites of such catalysts are ultimately downsized, which can afford high turnover frequencies (TOFs) for catalysis (*13*–*16*). Moreover, their heterogeneous structures could also avoid the solvent-dependent issue of molecular catalysis (*17*–*19*), increase the turnover numbers of active sites in aqueous solutions (*20*), and thus are suitable for integrating into devices for practical applications (*11*, *20*–*23*).

For a cycle of heterogeneous molecular catalysis, it usually takes place on (or with) the metal centers of the immobilized complexes. The geometric and electronic configurations of the complexes determine the chemisorption states of reactants/derived intermediates on the metal centers and the redox properties of the complexes, which govern the catalytic kinetics. Nevertheless, the comprehensive correlations between the structure and activity still have not been well clarified, and the quest for such knowledge has been the focus of many investigations. On the single molecular level, the structures of complexes on solid supports are well defined and can be altered through ligand control, with structural tuning realized in their first or second coordination spheres. In these variations, the mechanistic insights into the structural impacts on the geometric and electronic configurations of active sites are gained from molecularly discrete metal centers, which is relatively systematic and distinct from the insights from the studies of bulk or micro/nanosized metal catalysts focusing on their surfaces and interfaces made up of continuous metal centers (*24*). This not only derives a variety of novel catalysts but also provides the appropriate model platforms to approach the intrinsic structure-activity correlations of catalysts (*25*–*27*).

Here, we summarize recent progress in the structural tuning of TM complexes and present the inherent impacts of the structural variations on the activity in the context of heterogeneous molecular electrocatalysis. As far as we know, such perspective has not been discussed in other reviews recently reported. Specifically, the structural tuning is realized from first to second coordination spheres of complexes as presented in Fig. 1. The first spheres are directly bonded with metal centers, which could be tuned by changing the ligated atoms or introducing ancillary ligands at the axial coordination planes. The structural variations lead to direct impacts on the filling of electron orbitals in metal centers and the redox currents of heterogenized complexes. From another aspect, the second spheres refer to the functional groups appended on the ligands, which include adjacent metal centers, pendant groups, electron-donating/withdrawing, and conjugating moieties. Correspondingly, their modification allows the tuned chemisorption of reactants, shift of redox potentials of complexes, and even distinct catalytic cycles from traditional molecular catalytic cycles. Their impacts on key electrochemical reactions are discussed. These electrochemical reactions include the oxygen evolution reaction (OER), CO_2 reduction reaction (CO_2RR), and hydrogen evolution reaction (HER), which typically involve multiple protons and electrons transfer. Noting that the structures of molecular catalysts have the myriads of changes, we do not intend to provide a comprehensive summary but to

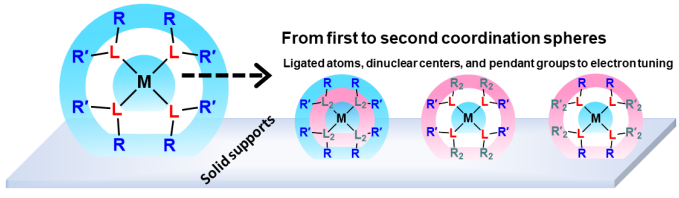

Fig. 1. Structural tuning of heterogeneous molecular catalysts. Tuning the structures of TM complexes with heterogeneous states from first to second coordination spheres.

[1]Institute of Advanced Synthesis, Northwestern Polytechnical University (NPU), Xi'an 710072, China. [2]Yangtze River Delta Research Institute of NPU, Taicang 215400, China. [3]School of Chemical and Biomedical Engineering, Nanyang Technological University, Singapore 637459, Singapore.
*Corresponding author. Email: wangxin@ntu.edu.sg

illustrate our viewpoints by using representative examples. Last, we propose the challenges and potential opportunities for developing efficient heterogeneous molecular catalysts based on structural tuning. We hope that through these efforts, better understanding on the intrinsic structure-activity correlations can be achieved and novel catalysts through rational structural design could be inspired.

TUNING OF LIGATED ATOMS IN FIRST COORDINATION SPHERE

From N to non-N atom ligation

In the first spheres of TM complexes, ligated atoms have direct impacts on the electronic structures of metal centers. The common ligated atoms are N atoms for a variety of molecular catalysts based on TM complexes. Toward the structural tuning of first spheres, neutral S, P, O, and C atom–based coordination can also be used to synthesize alternative complexes, which exhibit tunable activity because of the following two aspects: (i) These alternative atoms have different Lewis basicity from N as determined by atomic sizes and polarities; (ii) atoms such as S and P have larger sizes to generated prolonged coordination bonds with less steric effects. These two aspects allow the modulation of the interacting strength between ligands and metal centers, as well as the geometries of complexes. As a typical example, Pd complexes with triphosphine ligands have been known as homogeneous catalysts for CO_2-to-CO conversion in CH_3CN or *N*,*N*′-dimethylformamide (DMF) (*28*). When the ligated P atoms were replaced by N atoms (or C, O, S, and As atoms; Fig. 2A), the resultant Pd complexes turned to be catalytically inert (*29*). The redox characterizations indicated that the Pd triphosphine complexes exhibited two-electron reduction, while it changed to one-electron reduction with N (or C, O, S, and As) ligation in the same potential window. This implied a notable change in the electronic configurations of the complexes by the ligated atoms, which subsequently determined the catalytic activity. Ni bisdiphosphine complexes function as highly active catalysts for both HER and hydrogen oxidation reaction. With the formation of Ni-P coordination bonds, in the context of hydrogen oxidation, it provides appropriate pockets above the Ni-P coordination plane for the chemisorption of H_2 and heterolytic cleavage of H—H bonding between Ni center and the pendant group (*30*, *31*). Containing TM-S coordination bond, Co dithiolene complexes represent another type of typical HER catalysts (*32*–*34*). The complexes have different resonance forms (*35*). The first one contains enedithiolate and dithioketone, and the second one exhibits diradical character, where the ligated S atoms contain unpaired electrons (Fig. 2B). Theoretical studies indicated that, when the S atoms were substituted with N (or O) atoms, the participation probability of second resonance form increased. Correspondingly, there is a substantial drop of HER activity on the N (or O) atom coordinated complexes with analogous dithiolene structure.

The Ni centers embedded in graphene have been shown active for the conversion of CO_2 to CO, by which the maximum Faradic efficiency (FE) reached 99% at moderate overpotential (η) values in aqueous solutions (*36*, *37*). The embedded Ni centers can be ligated with N or C atoms to contain various possible active sites (*38*, *39*). Through density functional theory (DFT) calculations, Zhao and Liu (*38*) constructed a series of Ni-N_xC_y coordination moieties embedded into a molecularly sized graphitic cluster, i.e., Ni-C_3, Ni-C_4, Ni-N_1C_3, Ni-N_2C_2, Ni-N_3C_1, and Ni-N_4 moieties, as the model system (Fig. 2C). In particular, the authors showed that the charge capacity of Ni moieties was critical to activity. From N to C atom ligation, the Fermi energy level (E_F) of Ni moieties decreased under the charge-neutral condition. Namely, at the same E_F (i.e., same reduction potentials), the C atom ligation made the Ni moiety carry

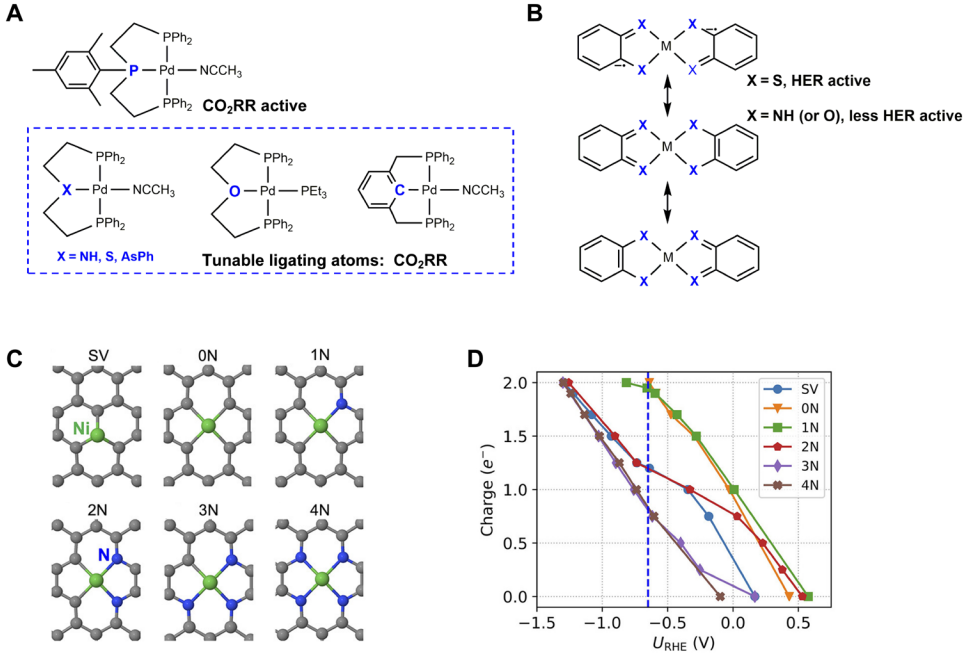

Fig. 2. Non-N ligation effect. (**A**) The Pd triphosphine complexes as CO_2RR catalysts and one P ligated atom was changed into O, C, N, S, and As atoms, respectively. (**B**) The S atom ligating-based complexes with different resonance states. (**C**) Various coordination moieties with a Ni center embedded in a molecular graphitic cluster. (**D**) Charge capacity dependence on the potential for *COOH at different Ni-based coordination moieties. (C and D) Reproduced with permission from (*36*). Copyright 2020 American Chemical Society. RHE, reversible hydrogen electrode. SV, single vacancy.

more amounts of negative charges, and the charge capacity reached optimal on the Ni-N_1C_3 moiety for deriving the highest activity (Fig. 2D). On this moiety, both the formation of H-bonds between CO_2 and solvent H_2O molecules and the interfacial electron transfer (IET) were facilitated, which promoted the chemisorption of CO_2 and generation of *COOH intermediate, as the key elemental steps in the CO_2RR cycle. This should intrinsically result from the different Lewis basicity between the ligated N and C atoms toward Ni centers.

Toward heterogeneous molecular catalysis, Ni bisdiphosphine complexes have been grafted onto carbon nanotubes (CNTs) through amide-based linkages. The resultant catalysts exhibited comparable HER activity to Pt catalysts in aqueous solutions (*40*–*42*). The amide-based linkages were constructed at the edge of the molecular plane of the complexes without affecting the Ni-P cores. The non-N ligation effect should be well maintained, with the mechanism being the same as that on the free-standing complexes. This linking strategy is common to the heterogenization of the active non-N ligated complexes onto graphitic carbon surfaces. Distinctively, Wang *et al.* (*11*) constructed the non–N atom–doped graphene, which was directly applied for ligating Co^{2+} ions. As shown in Fig. 3A, through hydrothermal synthesis, graphene was doped with various heteroatoms (i.e., O, N, and S atoms) in the forms of hydroxyl (HO—), carboxylic (COO—), pyridinic (N—), and sulfoxide (SO—) groups, respectively. These doped groups were verified to have the coordination ability to Co^{2+} ions, which generated Co coordination moieties with the tunable ligated atoms. From COO-/HO-Co^{2+}, N-Co^{2+} to SO-Co^{2+} ligation, the redox activity of $Co^{2+/3+}$ couple clearly increased (Fig. 3B), implying that the non-N ligation could influence the IET efficiency. The SO-Co^{2+} moiety also derived the most active sites with the highest TOFs for OER (Fig. 3C). In the process of clarifying the catalytic cycle on such Co centers, it was found that the SO groups of graphene can only occupy one coordination site of Co^{2+} ions because of the large steric effect of graphene. The rest of the coordination sites were reasonably occupied by the counterions of Co^{2+} ions or solvent molecules that can be labile for the chemisorption of reactants (i.e., HO^- ions). Before OER, the Co^{2+} ions were sequentially oxidized to Co^{3+} and Co^{4+} states, accompanied by the transfer of two and one HO^- (or H^+) ions, respectively. A HO^--Co^{4+} = O^{2-} intermediate was generated, and it led to the formation of O—O bond with side-on geometry on the Co centers (Fig. 3D).

Axial coordination

For CO_2RR and oxygen reduction reaction (ORR), porphyrins (Por), phthalocyanines (Pc), and other N-rich donor ligand–supported planar complexes represent a very important component of active molecular catalysts (*16*, *25*, *43*). For these complexes, their first spheres in the equatorial planes are structurally stable, while the axial positions can be coordinated by ancillary ligands. The increase of coordination number apparently changes the geometry of complexes, which is interdependent with the electronic configurations and thus determines the electrocatalytic activity. For instance, Cao *et al.* (*44*), in the investigation of FePc complexes toward ORR, verified that the axial coordination by pyridine (py) ligands rearranged the electron orbitals of complexes to decrease their spin states, which resulted in an enhanced ORR activity of FePc. Similarly, the axial coordination with N atoms also improved the ORR activity of the Fe-N_4 coordination moieties embedded in graphene (*45*, *46*). Jia *et al.* (*45*) suggested that the axial coordination reduced the filled electron numbers in e_g orbitals of Fe centers, which led to an appropriate end-on bonding between O_2 and Fe centers, facilitating the cleavage of O_2.

The effect of axial coordination was also verified in the investigation of CoPc complexes toward CO_2RR electrocatalysis. According to the study of Han *et al.* (*47*), the axial coordination of CoPc with

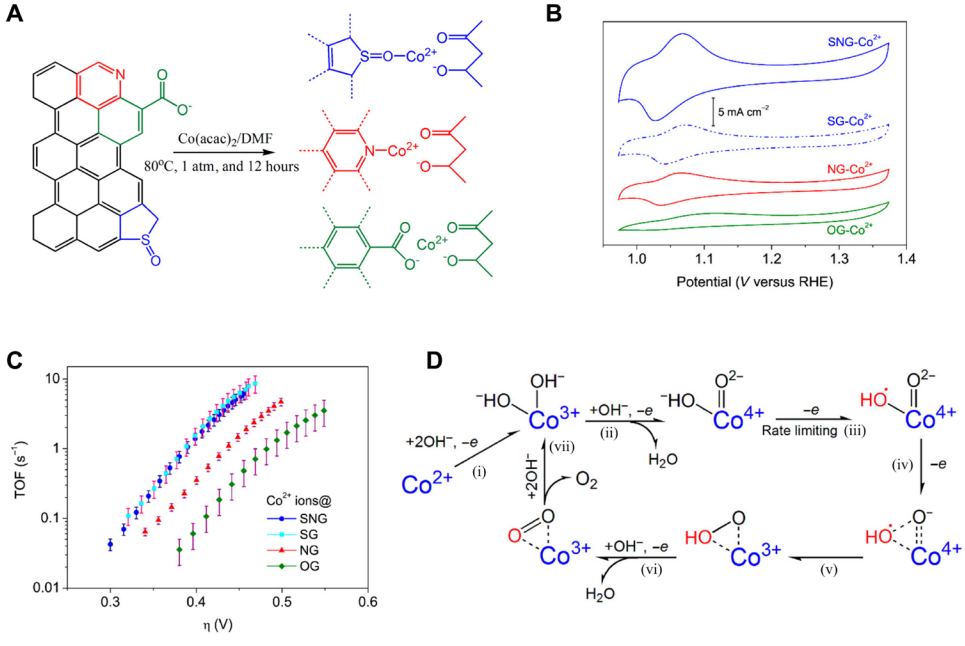

Fig. 3. A heterogenous molecular Co catalyst with tunable ligated atoms. (**A**) Immobilization of $Co(acac)_2$ onto S, N, O atom–doped graphene using a coordination tether. (**B**) Cyclic voltammograms of Co^{2+} ions on various graphene in 1 M KOH. (**C**) TOFs for OER. (**D**) A proposed OER cycle on the Co center. Reproduced with permission from (*11*). Copyright 2017 American Chemical Society. SNG, S/N/O-doped graphene; SG, S/O-doped graphene; NG, N/O-doped graphene; OG, O-doped graphene.

py ligands elevated the energy levels of dz^2 orbitals of Co centers (Fig. 4, A and B). The Co centers turned to be more nucleophilic, enabling stronger binding with the weak Lewis acidic C of CO_2 (*48*). The enhanced nucleophilicity of metal centers thus facilitated the chemisorption of CO_2 compared to the case of CoPc, which contributed to the decreased free energy difference for CO_2RR (Fig. 4C). Kramer and McCrory (*48*) also reported the catalytic enhancement in the CoPc with py coordination. They encapsulated CoPc into poly-4-vinylpyridine (P4VP) polymers with py of P4VP groups functioning as the axial ligands. Ongoing from CoPc to CoPc-py, the TOFs of Co centers for CO_2-to-CO conversion substantially increased from 0.6 to 4.8 s^{-1} [−1.2 V versus saturated calomel electrode (pH 4.7)]. In clarifying the CO_2RR cycle, it was even suggested that the py-based axial coordination changed the rate-determining step (RDS) (*49*). As shown in Fig. 4D, the kinetics of CO_2-to-CO conversion mainly depended on the chemisorption of CO_2 versus H^+ transfer (i.e., step i versus step iii) (*50*, *51*). The study of kinetic isotope effects showed that replacing H^+ with D^+ in the electrolytes decreased the catalytic currents on CoPc-py, while it did not affect the case in CoPc. This suggested that the RDS of CO_2RR was the chemisorption of CO_2 on CoPc, and it changed to H^+ transfer on CoPc-py.

Beyond these N atom–based ligations, Wang *et al.* (*12*) showed that the —SO and —COO groups doped in graphene can serve as the axial ligands for a planar complex of Co^{II}-2,3-naphthalocyanine (NapCo) through Co-O bonding. Toward CO_2RR, the NapCo-SO moiety exhibited a high FE value of 97% (η = 780 mV) in 0.1 M $KHCO_3$. Notably, its TOFs were about three times higher than those observed on the NapCo-COO moiety (Fig. 5, A and B). This phenomenon is very similar to that observed in the OER catalysis on the various heterogeneous Co centers as mentioned above (*11*). The increased TOFs could be attributed to the fact that (i) the axial —SO had a different charge transfer ability from NapCo compared to other cases and increased the intrinsic activity of Co centers (Fig. 5C) and (ii) the coordination promoted the IET efficiency between NapCo and graphene (Fig. 5D), which was likely because the axial coordination increased the electron coupling degrees between graphene and NapCo. The IET efficiency primarily determines whether the complexes can be redox active to mediate the catalysis. To further verify the axial coordination effect on IET, a series of S atom–based ligands (i.e., phenyl sulfoxide, phenyl sulfide, and their derivatives) were axially coordinated with the Co centers of PorCo complexes (*52*). Indeed, it reflected the variation of IET efficiency between complexes and graphene with the change of ligated atoms. It was found that the sulfide-based axial coordination was even more efficient in improving the IET efficiency on graphene surfaces than the case using sulfoxide-based axial coordination, and the IET efficiency was positively correlated to the apparent TOFs of Co centers for CO_2RR catalysis.

STRUCTURAL TUNING OF SECOND COORDINATION SPHERE

Dinuclear metal centers

The second spheres of complexes are outside the first spheres. Although they are relatively distant from metal centers without having chemical bonds, the structural tuning of second spheres can influence the catalytic activity of the complexes by appending various functional groups onto the ligands. One important tuning strategy is conversion of mononuclear metal center into dinuclear metal center, which was inspired by the metal centers of many natural metalloenzymes, such as hydrogenases with [Ni-Fe]/[Fe-Fe] centers

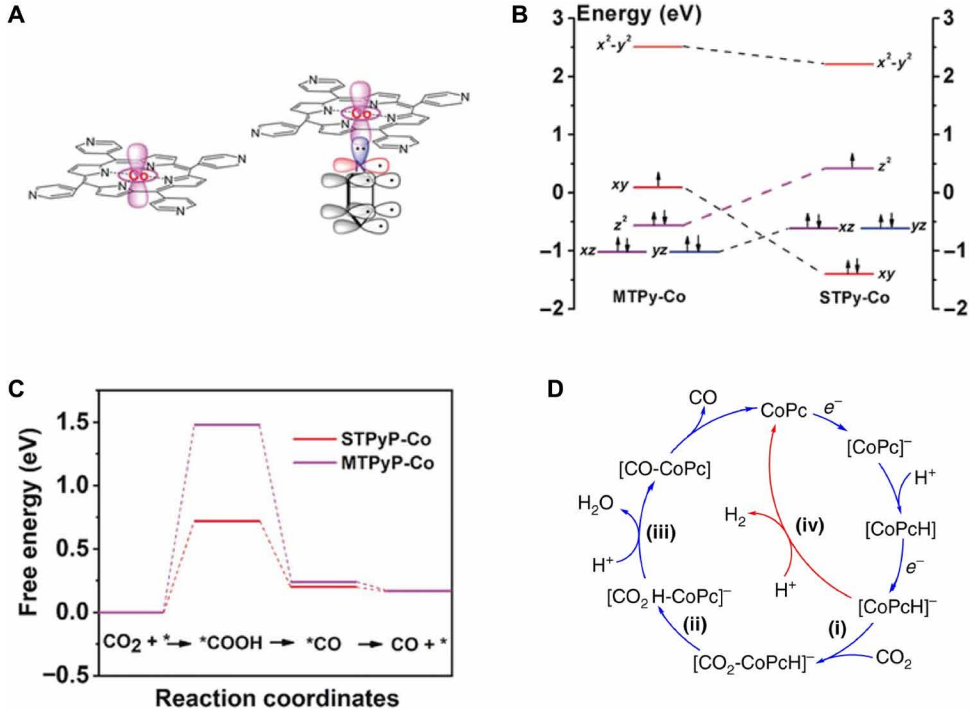

Fig. 4. Axial ligand effect. (**A**) Axial coordination by a py ligand on CoPc. (**B**) Co 3d orbital splitting by the axial coordination determined from multiplet fitting of Co L-edge absorption. (**C**) The free energy diagram for CO_2-to-CO conversion by CoPc with/without the py axial ligand. (**D**) A proposed cycle for CO_2-to-CO conversion by CoPc. (A to C) Reproduced with permission from (*47*). Copyright 2019 Wiley-VCH. (D) Reproduced with permission from (*49*). Copyright 2019 Nature Publishing Group. MTPy, molecular tetra(4-pyridyl); STPy, nanosheet of tetra(4-pyridyl).

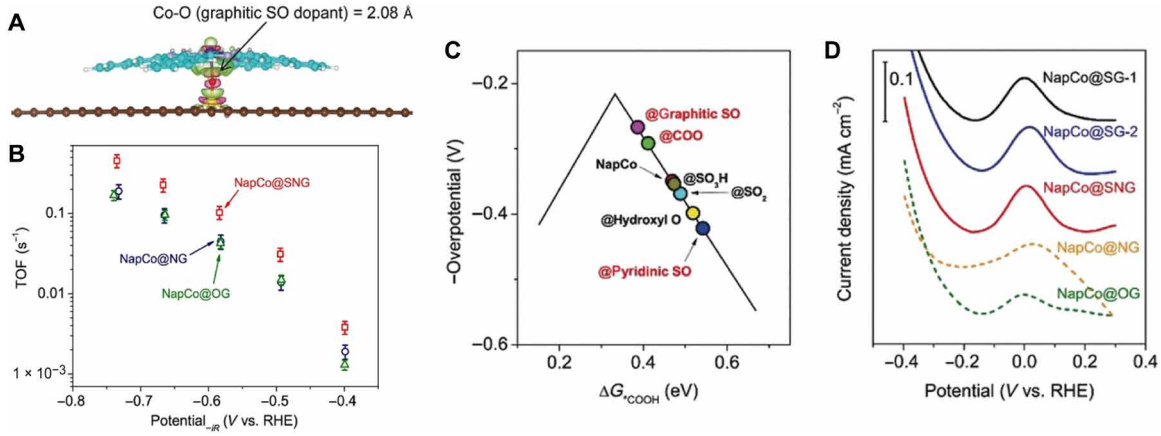

Fig. 5. Tuned electron transfer by axial ligands. (**A**) Charge density difference of NapCo axially bonded with the SO dopants of graphene. (**B**) TOFs of Co centers for CO_2-to-CO conversion on various NapCo. (**C**) Calculated overpotentials of CO_2RR on various NapCo as a function of ΔG^*_{COOH}. (**D**) Differential pulse voltammograms of various NapCo. Reproduced with permission from (*12*). Copyright 2019 Wiley-VCH.

and Cyt c oxidase with [Fe-Cu] centers (*53*–*55*). The dinuclear metal centers can coordinate with reactants through bridge geometry, distinct from mononuclear cases. Through such a configuration, reactants were electronically activated by both metal centers, or the chemisorbed intermediates were stabilized to facilitate subsequent elemental steps; thus, the enhanced activity can be achieved. The dinuclear Cu complexes with two (2-[bis(2-pyridinylmethyl)amino] ethyl)-ethane-1,2-diamine ligands have been reported for OER electrocatalysis (*56*). In an OER cycle, the dinuclear Cu centers had the bridge coordination geometry with —OH— species originating from activation of H_2O. Then, both Cu centers were oxidized from 2+ to 3+ state, resulting in the formation of O—O bonds between the bridge —OH— and one additional H_2O molecule, which was the RDS. The step was demonstrated to be more energetically favored on the dinuclear Cu centers compared to the mononuclear Cu centers, which can only have the linear coordination geometry with the oxygen species. The dinuclear Cu complexes with polypyridine-polyamide ligands are active ORR catalysts in acidic and neutral solutions (*57*). The study showed that at the reduction potentials, only one Cu center in the complex was reduced from 2+ to 1+ state to realize electron transfer with O_2. The other Cu center kept 2+ state, which should function to stabilize the chemisorption states of O_2 or the derived intermediates chemisorbed between Cu centers. Similarly, Ahmed *et al.* (*58*) synthesized a dinuclear Ni-Fe complex immobilized onto graphite through simple physisorption and tested it for HER catalysis. It also indicated that the HER was mediated through reduction of Ni^{2+} to Ni^{1+} center, while the Fe center stayed as 2+ state in the whole catalytic cycle (Fig. 6A).

Besides, other nontraditional synthetic strategies have been reported recently to achieve dinuclear metal centers with heterogeneous structures toward OER catalysis. Wang *et al.* (*59*) immobilized Ni^{2+} ions onto graphene through the ligation of SO dopants. The Ni centers were redox active with a pair of quasi-reversible $Ni^{2+/3+}$ redox peaks but were not intrinsically OER active. During the redox process, it was shown that free Fe^{3+} ions, which were intentionally introduced into the electrolyte, connected with the Ni centers through oxygen ligation and directly generated dinuclear Ni-Fe centers on the graphene surface. Correspondingly, the OER catalytic currents sharply increased by the formation of dinuclear Ni-Fe centers (Fig. 6B). The TOFs of Ni-Fe centers were even about two times higher than those of heterogeneous molecular Co centers reported previously (e.g., 0.53 s^{-1} versus 0.27 s^{-1} at η = 0.35 V) (*11*). The Pourbaix diagram analysis confirmed the typical cooperative catalysis on the dinuclear Ni-Fe centers. For the mononuclear Ni center, only one HO^- ion, as the reactant, was linearly coordinated, which did not provide sufficient chemisorbed reactants for OER. In contrast, each dinuclear Ni-Fe center linearly coordinated with two HO^- ions, and it contained one additional chemisorbed HO^- ion as the bridge ligand between the Ni and Fe centers (Fig. 6C). This coordination state in commencing the catalysis was analogous to those in natural hydrogenases, as well as the above stated dinuclear Cu complexes. More recently, Bai *et al.* (*60*) reported the synthesis of dinuclear Co-Fe centers based on a similar strategy, which were also intrinsically more active than corresponding mononuclear Co centers. Briefly, they synthesized single Co atoms within graphene through the pyrolysis of Co salts and 1,10-phenathroline. The ligands of single Co centers mainly included the N and C atoms of graphene. During the redox processes, it was suggested that parts of N and C ligated atoms were labile and replaceable by HO^- ions in alkaline electrolytes. The as-ligated HO^- ions functioned as the ligands to further connect with Fe^{3+} ions, thus generating the dinuclear Co-Fe centers.

Zhao *et al.* (*61*, *62*) reported a photochemical synthetic route to achieve Ir dinuclear centers on various metal oxides. The precursors of free-standing dinuclear Ir complexes can interact with Fe_2O_3, TiO_2, CeO_2, and WO_3 surfaces through the coordination between the terminal O atoms of metal oxides and Ir centers. However, the as-derived heterogeneous dinuclear Ir complexes were not catalytically active. The complexes were further treated with oxygen radicals, which were generated through ultraviolet beam, to remove the organic parts of the complexes. It resulted in a dinuclear Ir center interconnected by O atoms, as proposed in Fig. 6D (top). The structure was analogous to an atomic unit of IrO_2 (*61*). The dinuclear Ir center turned to be active for water oxidation, and the TOF at 1.23 V (versus reversible hydrogen electrode) was 2.6 times higher than the mononuclear Ir center synthesized following the same route. The DFT calculations suggested that both Ir centers were converted into highly oxidized Ir^{5+} states. Before binding to water, it underwent three proton-coupled electron transfer (PCET) steps to derive dinuclear moieties, which were sufficiently energetic to

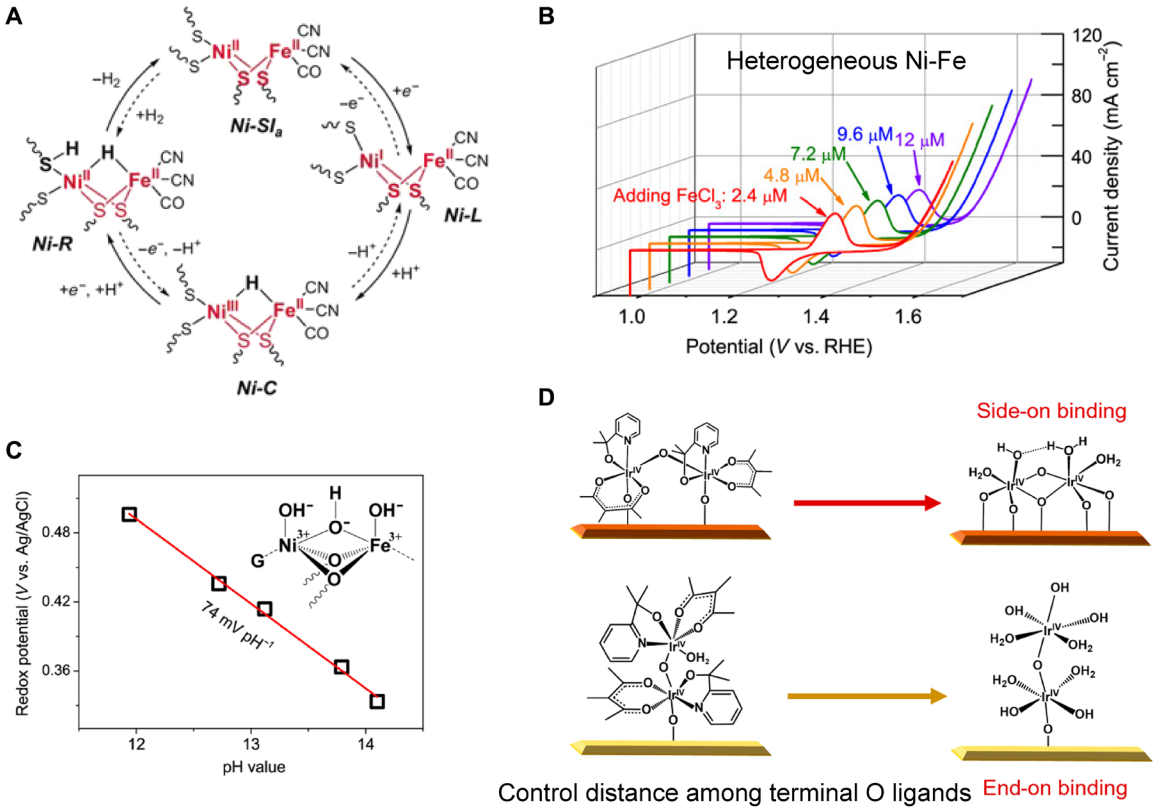

Fig. 6. Dinuclear metal centers. (**A**) A proposed HER cycle on LNi^{2+}Fe^{2+}Cp complexes. (**B**) Steady cyclic voltammograms suggested the gradual formation of Ni-Fe centers on graphene [heterogeneous Ni-Fe centers on heteroatoms doped graphene (HG-NiFe)] in 1 M KOH containing various contents of $FeCl_3$. (**C**) Pourbaix diagram of HG-NiFe. (**D**) Synthesis of side-on and end-on dinuclear Ir sites on metal oxides. (A) Reproduced with permission from (*58*). Copyright 2018 Wiley-VCH. (B and C) Reproduced with permission from (*59*). Copyright 2018 The American Association for the Advancement of Science. (D) Reproduced with permission from (*62*). Copyright 2018 American Chemical Society.

oxidize H_2O. For comparison, the mononuclear Ir centers only underwent two PCET steps to derive moieties that were less energetic. Besides, through controlling the distance among terminal O ligands or their surface amounts, the dinuclear Ir centers on metal oxides were turned from side-on to end-on immobilization geometry (Fig. 6D, bottom) (*62*). The centers with the end-on immobilization were geometrically more flexible than the ones with side-on immobilization because only one of the two Ir centers was bonded with the solid supports. This would decrease the steric effect of dinuclear Ir centers for interacting with reactants. The authors indicated that in the OER cycle, the side-on dinuclear Ir centers had the lower barriers both for chemisorption of H_2O and O_2 releasing compared to the end-on case.

In addition, molecular dinuclear metal sites have been incorporated into metal-organic frameworks (MOFs) (*63*, *64*). The continuous MOF-based structures grant the incorporated metal sites heterogeneous nature. Zhao *et al.* (*63*) showed that in ultrathin MOF nanosheets, Ni^{2+} and Co^{2+} ions were interconnected by O ligands provided by benzenedicarboxylic acids. Both the metal centers have open sites for the chemisorption of reactants and were applied as the OER catalyst. In a dinuclear Ni-Co center, it was found that there were partial electrons transferring from the Ni site to the Co site. This optimized the e_g filling states in the Ni sites, which turned to be energetic for interacting with oxygen species, and served as the main active sites. In the meantime, the redox potentials of Ni sites drastically decreased. The dinuclear Ni-Co center exhibited much higher OER activity compared to either single Ni or Co center with a similar coordination environment. More recently, the authors (*64*) showed that the dinuclear Ni-Co center, embedded in MOF-74, underwent a reversible structural evolution during OER catalysis. Upon applying potentials, a dinuclear center was successively converted into hydroxide [$Ni_{0.5}Co_{0.5}(OH)_2$] before the redox potential of metal centers and oxyhydroxide carrying oxygen vacancy ($V_o^{\bullet\bullet}$-$Ni_{0.5}Co_{0.5}OOH_{0.75}$) after metal redox and at OER potentials. The oxygen vacancy upshifted the antibonding states in $V_o^{\bullet\bullet}$-$Ni_{0.5}Co_{0.5}OOH_{0.75}$ to promote the chemisorption of oxygen species on the metal sites. The contained Ni site remained more OER active than the Co site. Compared to the case of single Ni site, the introduction of Co sites facilitates the generation of high-valence Ni site in oxyhydroxide, which served as the actual OER active site in catalytic turnovers.

Pendant group effect

The second spheres of complexes can be modified by appending various pendant groups above the metal centers. This establishes "reaction pockets" to stabilize the chemisorption states of reactants on metal centers or provide H^+-donor environments depending on the acidity of pendant groups. The strategy is best exemplified by tetraphenylporphyrin (TPP)–based complexes (*65*, *66*). In the investigation of CO_2RR on FeTPP, it was shown that the pendant group effect was influenced by pK_a (where K_a is the acid dissociation constant) values, relative positions, and numbers of the

appended groups (*67*–*70*). Margarit *et al.* (*67*) tailor-designed the pendant groups of FeTPP from phenol (PhOH), guanidinium (Gnd), to phenylsulfonic acid (3SA) groups with large difference in pK_a. As learned from the DFT calculations, with CO_2 chemisorbed onto the Fe centers, the pendant PhOH or Gnd groups also simultaneously interacted with CO_2 to form the intramolecular H-bonds (Fig. 7A). This stabilized the systems with the Gibbs free energy change (ΔG_H) of −6.62 and −2.13 kcal/mol, respectively, compared to the ones without pendant groups. Such intramolecular H-bonds did not form on the 3SA pendant groups. Because, in the used electrolyte (PhOH, pK_a of 18), the 3SA groups (pK_a = 3) were highly deprotonated to be negatively charged, it resulted in the electrostatic repulsion between the 3SA ions and TPP rings (or the anionic form of CO_2) negatively charged at the CO_2RR potentials. This destabilized the CO_2 adduct on the Fe centers. Accordingly, it derived the activity trend of CO_2-to-CO conversion: FeTPP-PhOH > FeTPP-Gnd > FeTPP-3SA (Fig. 7B). Although not favoring CO_2RR, the strong H^+ donor ability of 3SA groups was used to promote HER on FeTPP (*71*). The same authors also examined the impact of negative charges in the second sphere on the CO_2RR (*70*). They appended two pendant carboxylic groups, each located at one side of a FeTPP molecular plane. Both the pendant groups were deprotonated in the electrolyte of PhOH, and the resulting negative charges decreased the stability of chemisorbed CO_2 adducts, which were also negatively charged under the reduction potentials. Therefore, the as-configured FeTPP exhibited decreased activity compared to FeTPP with one-side pendant group, as well as the noncharged FeTPP.

Nichols *et al.* (*68*) showed that the relative positions of pendant amines on FeTPP were correlated to the stabilization of CO_2 adducts on Fe centers. Apparently, the relative positions of pendant groups should be neither too distant from nor too close to the metal centers. Among various analogous samples, the amines at the ortho positions of phenyl groups resulted in the stabilized CO_2 adducts and achieved the highest TOFs. Moreover, the authors simply added an electron-deficient molecule of bis(3,5-trifluoromethyl)-phenylurea into the electrolytes, and it also functioned as the pendant group for nickel cyclam in the CO_2RR catalysis (*72*). Despite the fact that the molecule was not appended on the cyclam ligand, its double amine sites still provided the H-bonding sites to the CO_2 adducts on the Ni centers and promoted the CO_2RR kinetics. Adversely, inappropriate positions of pendant groups could slow down the catalytic reaction. Chapovetsky *et al.* (*73*) investigated the Co complexes with aminopyridine ligands for CO_2 reduction. In the complexes, the H-bonding between the pendant amines and CO_2 adduct was energetically uphill (10.3 kcal mol^{-1}), involving a barrier of 15.2 kcal mol^{-1}. Instead, it was found that an intermolecular H-bond can be used to enhance the CO_2RR catalysis (Fig. 7C). In the selected electrolyte, 2,2,2-trifluoroethanol (TFE) was used as the proton donor for the protonation of CO_2. This acid also functioned as a bridge molecule connecting between the CO_2 adduct and pendant amines, with process downhill by −4.3 kcal mol^{-1} without barriers. In the CO_2RR cycle, such an intermediate state was proposed to be further protonated to generate CO, and this step was RDS. In addition, the intermolecular H-bonds were quantitatively controlled through increasing the number of pendant amines (Fig. 7D). In this process, the pK_a values of appended amines gradually increased and each amine was noncooperatively bonded to TFE. This further stabilized the CO_2 adducts and increased the local concentration of TFE above the Co centers, thus promoting the protonation of CO_2 adducts.

The pendant group effect can also change the CO_2RR cycle as reported by Rønne *et al.* (*74*) in the investigation of manganese bipyridine complexes containing pendant tertiary amines. Originally, on the pristine Mn centers without pendant amines, CO_2 was first chemisorbed followed by the formation of *COOH intermediate. This eventually led to the formation of CO product. In the presence of pendant tertiary amines, rapid delivery of H^+ near the Mn centers occurred since the pendant groups were considered as a Brønsted base having the protonation ability. Accordingly, the chemisorption of H^+ on the Mn centers turned to be facilitated compared to CO_2, and it primarily generated [Mn-H] sites. The chemisorption

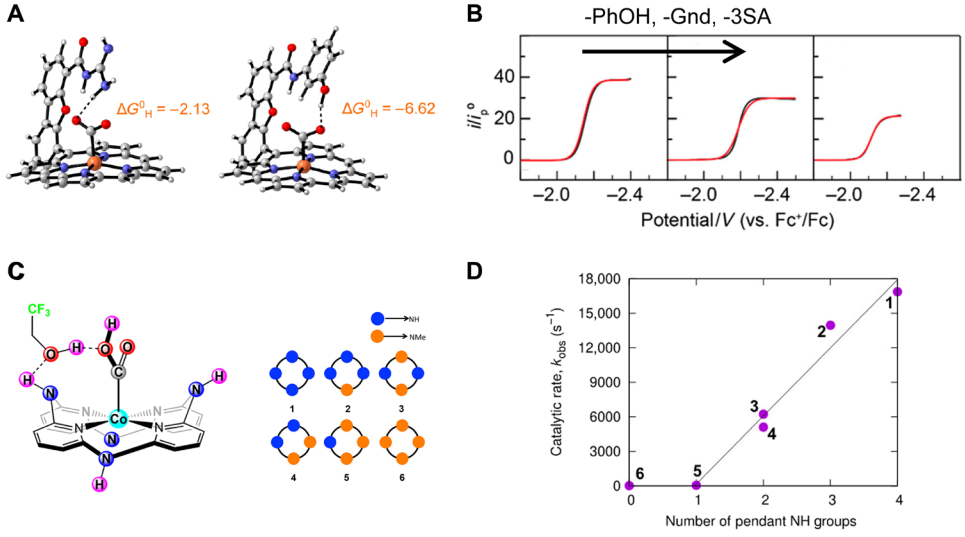

Fig. 7. Pendant group effect. (**A**) FeTPP-Gnd (left) and FeTPP-PhOH (right) with CO_2 adduct. (**B**) Plateau analysis of CO_2RR by FeTPP-PhOH, FeTPP-Gnd, and FeTPP-3SA. (**C**) The intermolecular H-bonds between TFE and Co complexes. The number of pendant amines in complexes was tuned. (**D**) The dependence of k_{obs} on the number of pendant amines in the Co complexes. (A and B) Reproduced with permission from (*67*). Copyright 2019 American Chemical Society. (C and D) Reproduced with permission from (*73*). Copyright 2018 American Chemical Society.

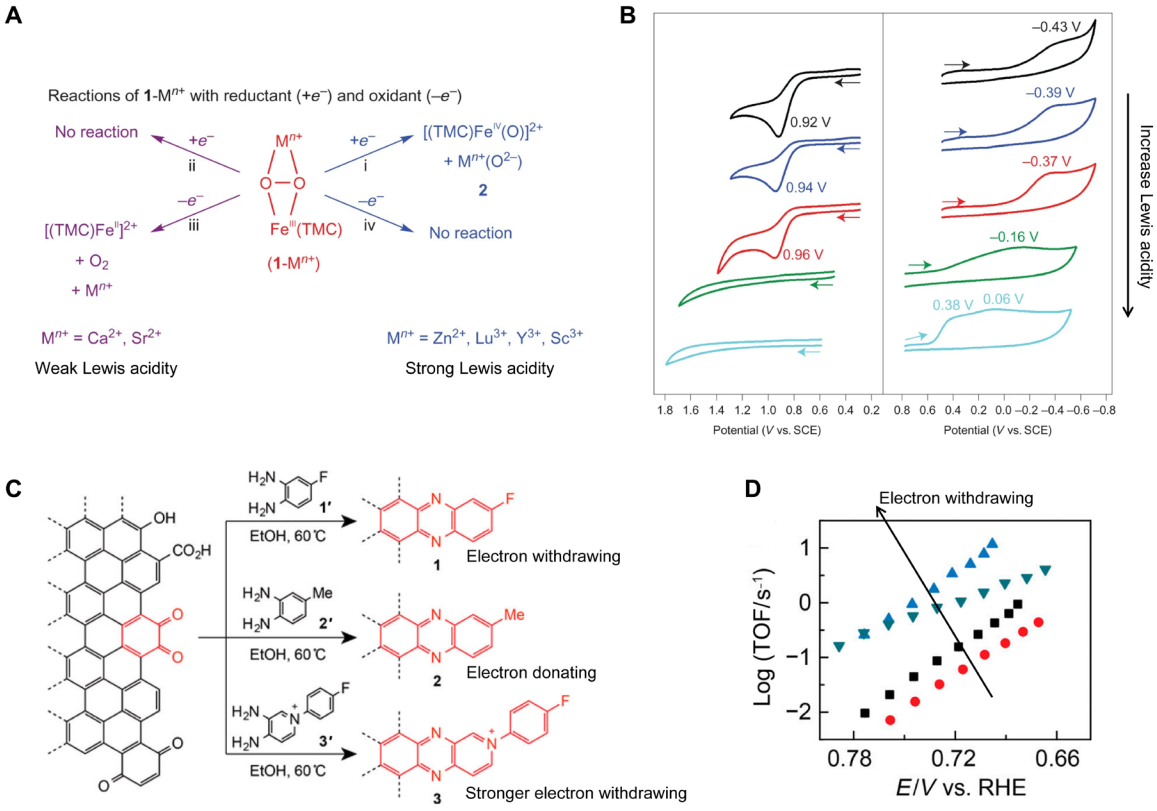

Fig. 8. Electron withdrawing/donating effect. (**A**) Effect of the Lewis acidity of redox-inactive metal ions on the reactions of 1-M^{n+} with reductant ($+e^-$) and oxidant ($-e^-$). (**B**) Cyclic voltammograms of **1** (black) and **1**-M^{n+} [M^{n+} = Sr^{2+} (blue), Ca^{2+} (red), Zn^{2+} (green), and Sc^{3+} (cyan)] with $1e^-$ oxidation (left) and $1e^-$ reduction (right) in MeCN at −20°C. (**C**) Condensation of *o*-phenylenediamine derivatives with *o*-quinone sites at graphene graphene. (**D**) Tafel plots of per site activity versus potential for **1** (black), **2** (red), **3** (blue), and polycrystalline Ag (green). (A and B) Reproduced with permission from (*77*). Copyright 2014 Nature Publishing Group. (C and D) Reproduced with permission from (*80*). Copyright 2015 American Chemical Society.

of CO_2 was then realized through interacting with the [Mn-H] sites to derive —OCHO on the Mn centers, which is the precursor of HCOOH. Thus, the catalytic product was tuned from CO to HCOOH. We noted that the pendant group effect in TPP-based or other analogous complexes were mainly revealed in the investigations of homogeneous catalysis (*75*), while they have been rarely reported in the heterogeneous states. Indeed, the complexes with pendant groups are structurally complicated or have large steric effects to hinder the realization of their heterogeneous structures. Among the limited examples, Maurin and Robert (*76*) replaced one phenyl group in FeTPP with a pyrene unit and successfully immobilized the complex onto CNT through pyrene moiety based on π-π interactions. In the CoPc/polymer systems proposed by McCrory and colleagues (*48*, *49*), it suggested the possible involvement of pendant group effect; namely, some random py groups on polymer chains could be located above the equatorial plane of CoPc, which facilitated the chemisorption of CO_2 and H^+ transfer toward the CO_2 adducts.

Electron withdrawing and donating moieties

Learning from the natural oxygen-evolving complex (OEC) of photosystem II, the second spheres can be appended with electron-withdrawing/donating moieties to improve catalytic activity. The OEC is made up of manganese-calcium-oxygen cluster (Mn_4CaO_5). The Ca^{2+} ion is redox inactive but has certain Lewis acidity to optimize the redox potentials of the adjacent Mn-oxo active sites, which is thus critical for catalytic activity. This has been verified by various studies in which various synthetic complexes are modified through incorporating redox-inactive metal ions with various Lewis acidities to mimic the OEC (*77*–*79*). A typical example is the complex of $[(TMC)Fe^{II}]^{2+}$ (TMC = 1,4,8,11-tetramethyl-1,4,8,11-tetraazacyclotetradecane) (*77*), which was bonded to O_2 under photoirradiation in the presence of M^{n+} (M^{n+} = Sr^{2+}, Ca^{2+}, Zn^{2+}, Lu^{3+}, Y^{3+}, and Sc^{3+}, respectively) to derive the M^{n+} and peroxo bound Fe^{III} complexes (i.e., $[(TMC)Fe^{III}(\mu,\eta^2{:}\eta^2\text{-}O_2)]^+$-$M^{n+}$, **1**-$\mathbf{M}^{n+}$; Fig. 8A). The peroxo species was further either reduced to O^{2-} species or oxidized to O_2 for realizing ORR and OER, respectively. With increasing the Lewis acidities of M^{n+}, which can draw more electron density from the active sites, the oxidation potential of peroxo species of **1**-$\mathbf{M}^{n+}$ increased, while the reduction potential decreased (Fig. 8B). This indicated the opposite impacts of electron withdrawing/donating on the catalysis of OER and ORR. In addition, Fukushima *et al.* (*80*) investigated the same effects in the heterogeneous molecular catalysis for ORR. They condensed *o*-phenylenediamine derivatives with *o*-quinone moieties at graphene edges to derive a phenylenediamine moiety as the active sites (Fig. 8C). The electron withdrawing (i.e., -fluoro and -fluoro-connected pyridinum) and donating (i.e., -methyl) groups were appended onto the phenylenediamine moiety, respectively. The electron donation clearly led to high TOFs of active sites, which followed the same trend of ORR activity for those above **1**-$\mathbf{M}^{n+}$ complexes (Fig. 8D).

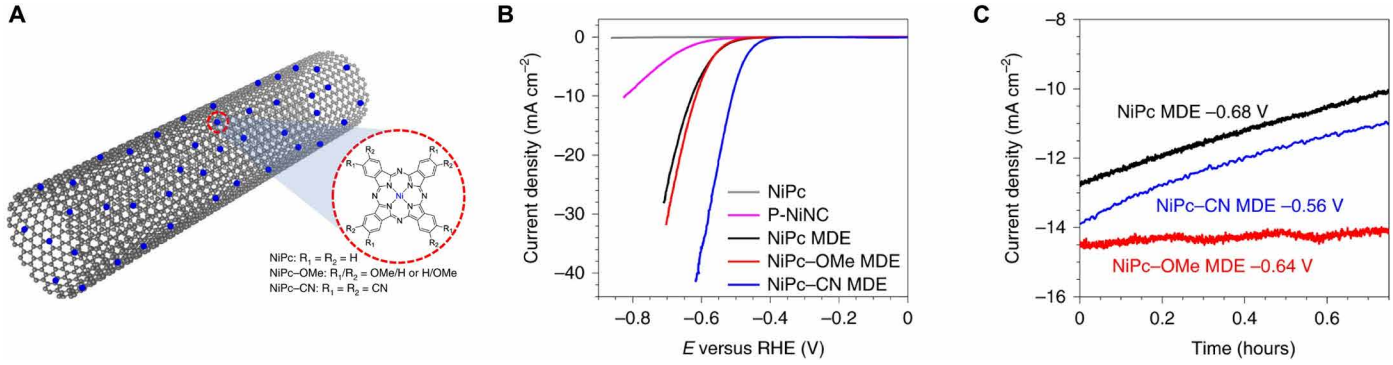

Fig. 9. Heterogeneous NiPc appended with electron withdrawing/donating groups. (**A**) Various NiPc immobilized on CNT. (**B**) Linear scanning voltammograms of NiPc-based catalysts in CO_2-saturated 0.5 M $KHCO_3$. (**C**) Chronoamperometry of NiPc/CNT at −0.68 V, NiPc-CN/CNT at −0.56 V, and NiPc-OMe/CNT at −0.64 V. The potentials were referenced against RHE. Reproduced with permission from (*81*). Copyright 2020 Nature Publishing Group.

By anchoring NiPc onto CNT via π-π stacking, Zhang *et al.* (*81*) found that appending cyano (-CN) groups, as the strong electron-withdrawing groups, onto Pc ligands decreased the η for catalyzing CO_2 to CO (Fig. 9, A and B). Mukerjee and colleagues (*45*, *82*) suggested that in such a variation, the e_g energy levels of metal centers of complexes downshift with electron withdrawing, accompanied with anodic shifts of redox potentials of metal centers. As the redox of metal centers mediated the catalysis, the η decreased accordingly (*83*). This could be feasible for both CO_2RR and ORR, as well as other reduction processes [we noted that in some cases, the coordination of CO, H^+, or/and intermediates/products is related to the electron density of metal centers, which could affect the kinetics of CO_2RR, as discussed by Barlow and Yang (*84*); this complicates the redox-mediated mechanism but does not conflict with the above general correlation between electron density of metal centers and η]. In Liang's work, it is indeed observed that the redox potentials of NiPc anodically shifted to high potentials with appending the -CN groups. The redox of NiPc occurred before CO_2RR potentials, suggesting the redox-mediated catalytic mechanism. This similar phenomenon was also observed in CoPc/CoPc-CN–based heterogeneous CO_2RR catalysis (*85*). Unfortunately, NiPc and NiPc-CN on CNT exhibited poor durability, especially at the high reduction potentials (Fig. 9C). Even the classical CoPc/CNT system was reported to be catalytically durable for only about 1 hour (*86*). Structural analysis showed that the Pc ligands were hydrogenated under the reduction environments, leading to demetallization of complexes and loss of molecular active sites with the formation of metals and/or metal oxides (*81*, *86*). The issue was addressed by appending electron-donating groups, methoxy (-OMe), onto the Pc ligands, at the cost of increase overpotential compared to that on pristine NiPc/CNT. As gained from x-ray absorption spectroscopy data, the appended -OMe moieties could increase the reduction potentials of NiPc, which could hinder the hydrogenation of Pc ligands and increase the structural stability of NiPc. The NiPc-OMe/CNT can be kept durable at 150 mA cm^{-2} for 40 hours in an assembled gas diffusion layer electrode. Appending of amine groups (-NH_2) onto the Pc ligands of CoPc for electron donating also improved the catalytic durability of CO_2-to-methanol conversion, which lasted for 12 hours without a clear drop of catalytic selectivity (*86*). Such an electron donating effect thus shed light on the practical application of heterogeneous molecular catalysis based on the Pc complexes.

In the DFT study, the theoretical η values on NiPc and its derivatives, however, were inversely correlated with the experimental results (*81*). Such a contradiction might be attributed to the structural variation of NiPc during the redox of NiPc. Indeed, the structure of the reduced NiPc could contain different hydrogenated and charged states (*87*). Besides, in the heterogeneous states, NiPc can be conjugated with graphitic carbon-based supports. This further complicates the molecular structures of reduced NiPc (details are discussed in the following part), which currently might be difficult to be fully reflected by current DFT models.

Electron conjugation effect

To support free complexes, graphitic carbon has been widely used because of its high supporting capacity, good conductivity, and structural stability (*88*, *89*). Notably, graphitic carbon contains highly conjugated π electrons, which can stabilize additional electrons introduced externally. This feature can change the redox behaviors of the supported complexes and allow the tuning of their catalytic properties. Garrido-Barros *et al.* (*90*) synthesized $[(L)Cu^{2+}]^{2-}$ [L = *o*-phenylenebis(oxamidate)] complexes, $\mathbf{1}^{2-}$, which emerged as a representative molecular catalyst for OER in alkaline solutions (Fig. 10A). In an OER cycle, $\mathbf{1}^{2-}$ was oxidized to $[(L)Cu^{3+}]^{1-}$ ($\mathbf{1}^{1-}$), followed by the generation of $[(L^+)Cu^{3+}(OH)]^-$ as the active site to commence the catalysis. In these redox steps, it involved the oxidation of phenyl rings of $\mathbf{1}^{2-}$, which was reversible, to determine the generation of active site. On the phenyl groups of $\mathbf{1}^{2-}$, the authors appended pyrene groups to derive the $[(L_{py})Cu^{2+}]^{2-}$ [L = 4-pyrenyl-1,2-phenylenebis(oxamidate)], $\mathbf{2}^{2-}$. Compared to the $\mathbf{1}^{2-}/\mathbf{1}^{1-}$ couple, the redox potential of $\mathbf{2}^{2-}$ to $\mathbf{2}^{1-}$ was cathodically shifted by 130 mV, which was realized through the oxidation of pyrene groups (i.e., the generation of $[(L_{py}^+)Cu^{2+}]^{1-}$, Fig. 10B). This verified that the conjugated π electrons of pyrene moiety stabilized the introduced electrons. Afterward, the active sites of ($[(L_{py}^+)Cu^{3+}(OH)]^{1-}$) were derived to oxidize HO^- ions. The TOF_{max}, based on the foot of the wave analysis, achieved 128 s^{-1} on $\mathbf{2}^{2-}$ versus 6.2 s^{-1} on $\mathbf{1}^{2-}$ (Fig. 10C), demonstrating the significant impacts of electron-conjugated effects on the OER catalysis. Taking advantage of the effect, $\mathbf{2}^{2-}$ was immobilized onto graphene (**G**) by π-π stacking. The π conjugation degree in graphene was much higher than that in pyrene moiety. Accordingly, the TOF_{max} further increased to 540 s^{-1} on **G**-$\mathbf{2}^{2-}$, and even in the case of **G**-$\mathbf{1}^{2-}$, the TOF_{max} increased to 320 s^{-1}. In a series of work of Surendranath and colleagues (*80*, *91*, *92*), the pyrazine moieties

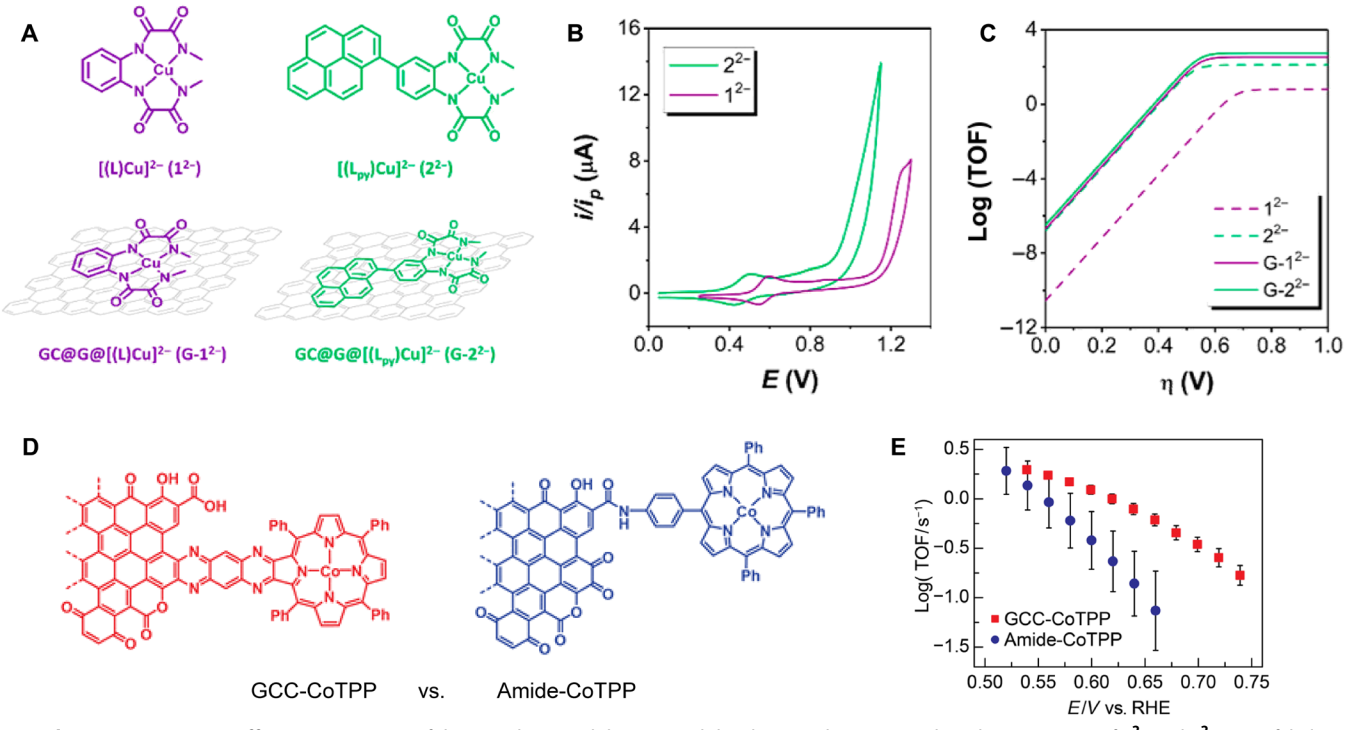

Fig. 10. Electron conjugation effect. (**A**) Structures of the complexes and those immobilized on graphene. (**B**) Cyclic voltammograms of $\mathbf{1}^{2-}$ and $\mathbf{2}^{2-}$. (**C**) Tafel plots for $\mathbf{1}^{2-}$, $\mathbf{2}^{2}$, **G-1**$^{2-}$, and **G-2**$^{2-}$. (**D**) Structures of GCC-CoTPP and Amide-CoTPP. (**E**) TOFs for ORR on GCC-CoTPP and Amide-CoTPP. (A to C) Reproduced with permission from (*90*). Copyright 2017 American Chemical Society. (D and E) Reproduced with permission from (*91*). Copyright 2019 American Chemical Society.

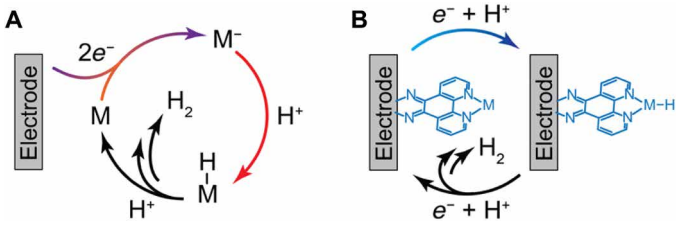

Fig. 11. Tuned catalytic mechanism by electron conjugation. (**A**) Complexes mediate HER through stepwise pathways. (**B**) Graphene-conjugated complexes for HER through concerted proton and electron transfer. Reproduced with permission from (*93*). Copyright 2019 American Chemical Society.

served as the covalent linkages between graphene edges and complexes [e.g., CoTPP; Fig. 10D (*91*)]. The electrons between these moieties are highly conjugated to derive graphite-conjugated catalyst-CoTPP (GCC-CoTPP). For comparison, a control sample was included where CoTPP complexes were attached to graphene edges through nonconjugated amide linkages (Amide-CoTPP). Toward ORR, the TOFs of Co centers in GCC-CoTPP were almost one order of magnitude higher than those in Amide-CoTPP (Fig. 10E). The result again confirmed the π conjugation effect in the improvement of catalytic activity.

It is accepted that the catalysis on complexes commonly adopts the redox-mediated mechanism. It contains multiple elemental steps, which proceed depending on the redox of complexes (Fig. 11A). In the work of Jackson *et al.* (*93*), it is suggested that the electron conjugation effect can intrinsically change the mechanism of molecular catalysis on graphene by eliminating access to stepwise redox mediation pathways. Because of the strong interfacial electron conjugation established by pyrazine linkages, the energy difference between complexes and graphene was eliminated; thus, the redox of metal complex never occurred. This is analogous to that on metallic catalysts, where the redox of surface atoms usually does not occur. Instead, the IET, mediated by graphene and complexes, is directly realized on the reactants once they chemisorb on the complexes at applied potentials (Fig. 11B) (*22*, *93*). The concerted chemisorption of reactants and IET can avoid some elemental steps in molecular catalysis, some of which would have been RDSs with high barriers otherwise.

CONCLUSION AND PERSPECTIVE

This review summarized various strategies on structurally tuning of TM complex–based heterogeneous molecular catalysts for efficient electrocatalytic applications such as H_2O splitting and O_2/CO_2 reduction. The tunable structures of molecular catalysts also provide appropriate model systems to investigate the structure-activity correlations of catalysts through a combination of activity measurement, operando structural analysis, and DFT calculations. Through these insights, it is expected that the application of these structural tuning strategies can be extended to discover more active and stable heterogeneous molecular catalysts.

On the basis of tailored design from first coordination sphere to second coordination sphere, it revealed different electronic and geometric impacts on the redox of complexes, chemisorption of reactants, and catalytic cycles toward achieving high catalytic activity. For the first spheres, their structural variations were realized by varying ligated atoms or appending ancillary ligands. This directly changed the electron filling states in metal centers and subsequently modulated the intrinsic activities. In parallel, it was suggested that

the ligated atoms on the solid supports served as the linkages for complexes and determined the IET efficiency between the immobilized complexes and electrodes. Adjacent to the first spheres, the tuning of second spheres of complexes have been shown to optimize the catalytic activity of complexes through the following effects: (i) to stabilize the chemisorbed reactants on metal centers through bridge binding with appended pendant groups or adjacent metal centers; (ii) to facilitate the H^+ transfer by providing local H^+ sources; and (iii) to change the redox properties of metal centers with electron withdrawing, donating, and conjugating to effectively decrease η values of catalysis.

Despite the above progress, there are still challenges remaining to be addressed, and they can basically be converged to three aspects. First, the above-stated structural tuning strategies still have not been readily used for practical heterogeneous molecular catalysts, especially in the cases of constructing the dinuclear metal centers and pendant groups, because of the relatively complicated structures of such coordination spheres with large steric effects for the heterogenization processes. For instance, to append pendant groups onto complexes, it needs to control the molecular linking between complexes and solid supports simultaneously, which require multiple synthetic steps and is difficult (*94*). One possible way to address this challenge is to modify solid supports, as proposed above (*11*, *12*, *48*, *49*), so that they could directly function as parts of ligands with linking ability or pendant moieties toward the immobilized complexes. This might save some synthetic steps for appending multiple functional groups onto complexes and simplify their structures in achieving the stable heterogeneous configurations. Besides, it might be promising to explore electrochemical and photochemical methods to achieve such active heterogeneous molecular catalysts with complicated and novel structures, which can be more convenient compared to traditional synthetic strategies (*59*–*62*). The second issue is the low loading of complexes on solid supports, which was reported at the magnitude of 2 to 20 nmol cm^{-2} (*20*, *91*), although the high TOFs have been achieved. This can be resolved by activation of the supports or enlarging specific surface area through introducing structural defects, as well as developing more efficient molecular linkages between complexes and supports. In addition, another resolution that might ultimately resolve the loading issue is the construction of interconnected multiple dimensional networks or multiple layers of complexes, such as MOF- and covalent organic framework (COF)–based solid supports (*95*–*97*). Following this strategy, Chang and colleagues (*96*, *97*) reported that the surface loading amount of CoTPP on electrodes reached up to 250 nmol cm^{-2}, which was about one to two magnitude higher than the ones of discrete complexes. However, it brought up an issue of reduced IET efficiency concurrently. For CoTPP embedded in COFs (*96*), only 4% of Co centers exhibited the redox features on the electrode. The other Co centers were redox inactive, suggesting that they did not have the electron transfer ability with the electrode and cannot serve as the efficient active sites. This is likely because the constructed networks either increased the electron transfer distance or decreased the electron coupling degree between complexes and electrodes. It is essential to develop conductive COFs/MOFs for supporting complexes, such as those networks interconnected with the linkers containing π-conjugated structures or reversible redox couples as the mediators for IET (*98*–*100*). Last, it is important to identify the structural durability of molecular active centers under turnover conditions. The applied potentials are commonly not moderate, which could reduce or oxidize some vulnerable ligands and damage the whole molecular catalytic structures. This could significantly decrease TOFs or lead to false structure-activity correlations of molecular catalysis. For instance, cobalt diamine-dioxime complexes were reported as active HER catalysts in acidic aqueous solutions (*101*), while Kaeffer *et al.* (*102*) showed that, for such complexes in the free-standing state, the imine-based ligands were decomposed at reduction potentials and the Co ions were aggregated into nanoparticles on the electrode surface, which actually functioned as the HER active sites. Note that the as-derived nanoparticles were metastable, which can be redecomposed or desorb during rinsing of the electrodes. Some metal complexes were even reported to have reversible structural transformation into metals or metal oxides/hydroxides during catalysis (*64*, *103*). Therefore, identifying the structural decomposition of molecular might not be easy. To promote the structural durability of molecular catalysis, it is important to (i) select ligands with robust backbones (e.g., ligands with conjugated backbones) or change the redox potentials of ligands based on appending electron donating/withdrawing moieties to not overlap with catalytic potentials and (ii) strengthen the immobilization force between solid supports and complexes. If these challenges are successfully addressed, then heterogeneous molecular catalysts will see real potential for practical applications in electrochemical energy conversion.

REFERENCES AND NOTES

1. N. S. Lewis, D. G. Nocera, Powering the planet: Chemical challenges in solar energy utilization. *Proc. Natl. Acad. Sci. U.S.A.* **103**, 15729–15735 (2006).
2. J. Schmidt, K. Gruber, M. Klingler, C. Klöckl, L. Ramirez Camargo, P. Regner, O. Turkovska, S. Wehrle, E. Wetterlund, A new perspective on global renewable energy systems: Why trade in energy carriers matters. *Energ. Environ. Sci.* **12**, 2022–2029 (2019).
3. J. Gong, C. Li, M. R. Wasielewski, Advances in solar energy conversion. *Chem. Soc. Rev.* **48**, 1862–1864 (2019).
4. A. Navarrete, G. Centi, A. Bogaerts, Á. Martín, A. York, G. D. Stefanidis, Harvesting renewable energy for carbon dioxide catalysis. *Energ. Technol.* **5**, 796–811 (2017).
5. Z. Yang, J. Zhang, M. C. W. Kintner-Meyer, X. Lu, D. Choi, J. P. Lemmon, J. Liu, Electrochemical energy storage for green grid. *Chem. Rev.* **111**, 3577–3613 (2011).
6. T. M. Gür, Review of electrical energy storage technologies, materials and systems: Challenges and prospects for large-scale grid storage. *Energy Environmen. Sci.* **11**, 2696–2767 (2018).
7. Z. Yan, J. L. Hitt, J. A. Turner, T. E. Mallouk, Renewable electricity storage using electrolysis. *Proc. Natl. Acad. Sci. U.S.A.* **117**, 12558–12563 (2020).
8. K. Scott, Chapter 1 Introduction to electrolysis, electrolysers and hydrogen production, in *Electrochemical Methods for Hydrogen Production* (The Royal Society of Chemistry, 2020), pp. 1–27.
9. Y. Zheng, J. Wang, B. Yu, W. Zhang, J. Chen, J. Qiao, J. Zhang, A review of high temperature co-electrolysis of H_2O and CO_2 to produce sustainable fuels using solid oxide electrolysis cells (SOECs): Advanced materials and technology. *Chem. Soc. Rev.* **46**, 1427–1463 (2017).
10. P. De Luna, C. Hahn, D. Higgins, S. A. Jaffer, T. F. Jaramillo, E. H. Sargent, What would it take for renewably powered electrosynthesis to displace petrochemical processes? *Science* **364**, eaav3506 (2019).
11. J. Wang, X. Ge, Z. Liu, L. Thia, Y. Yan, W. Xiao, X. Wang, Heterogeneous electrocatalyst with molecular cobalt ions serving as the center of active sites. *J. Am. Chem. Soc.* **139**, 1878–1884 (2017).
12. J. Wang, X. Huang, S. Xi, J.-M. Lee, C. Wang, Y. Du, X. Wang, Linkage effect in the heterogenization of cobalt complexes by doped graphene for electrocatalytic CO_2 reduction. *Angew. Chem. Int. Ed.* **58**, 13532–13539 (2019).
13. M. Rakowski Dubois, D. L. Dubois, Development of molecular electrocatalysts for CO_2 reduction and H_2 production/oxidation. *Acc. Chem. Res.* **42**, 1974–1982 (2009).
14. J. M. Le, K. L. Bren, Engineered enzymes and bioinspired catalysts for energy conversion. *ACS Energy Lett.* **4**, 2168–2180 (2019).
15. J. D. Blakemore, R. H. Crabtree, G. W. Brudvig, Molecular catalysts for water oxidation. *Chem. Rev.* **115**, 12974–13005 (2015).
16. C. Costentin, M. Robert, J.-M. Savéant, Catalysis of the electrochemical reduction of carbon dioxide. *Chem. Soc. Rev.* **42**, 2423–2436 (2013).

17. G. H. Gunasekar, J. Shin, K.-D. Jung, K. Park, S. Yoon, Design strategy toward recyclable and highly efficient heterogeneous catalysts for the hydrogenation of CO_2 to formate. *ACS Catal.* **8**, 4346–4353 (2018).
18. B. Reuillard, K. H. Ly, T. E. Rosser, M. F. Kuehnel, I. Zebger, E. Reisner, Tuning product selectivity for aqueous CO_2 reduction with a Mn(bipyridine)-pyrene catalyst immobilized on a carbon nanotube electrode. *J. Am. Chem. Soc.* **139**, 14425–14435 (2017).
19. I. Roger, M. A. Shipman, M. D. Symes, Earth-abundant catalysts for electrochemical and photoelectrochemical water splitting. *Nat. Rev. Chem.* **1**, 0003 (2017).
20. E. S. Andreiadis, P.-A. Jacques, P. D. Tran, A. Leyris, M. Chavarot-Kerlidou, B. Jousselme, M. Matheron, J. Pécaut, S. Palacin, M. Fontecave, V. Artero, Molecular engineering of a cobalt-based electrocatalytic nanomaterial for H_2 evolution under fully aqueous conditions. *Nat. Chem.* **5**, 48–53 (2013).
21. J. D. Blakemore, A. Gupta, J. J. Warren, B. S. Brunschwig, H. B. Gray, Noncovalent immobilization of electrocatalysts on carbon electrodes for fuel production. *J. Am. Chem. Soc.* **135**, 18288–18291 (2013).
22. M. N. Jackson, S. Oh, C. J. Kaminsky, S. B. Chu, G. Zhang, J. T. Miller, Y. Surendranath, Strong electronic coupling of molecular sites to graphitic electrodes via pyrazine conjugation. *J. Am. Chem. Soc.* **140**, 1004–1010 (2018).
23. Y. Jiao, Y. Zheng, M. Jaroniec, S. Z. Qiao, Design of electrocatalysts for oxygen- and hydrogen-involving energy conversion reactions. *Chem. Soc. Rev.* **44**, 2060–2086 (2015).
24. C. Xie, Z. Niu, D. Kim, M. Li, P. Yang, Surface and interface control in nanoparticle catalysis. *Chem. Rev.* **120**, 1184–1249 (2020).
25. J. Bonin, A. Maurin, M. Robert, Molecular catalysis of the electrochemical and photochemical reduction of CO_2 with Fe and Co metal based complexes. Recent advances. *Coord. Chem. Rev.* **334**, 184–198 (2017).
26. J. R. McKone, N. S. Lewis, H. B. Gray, Will solar-driven water-splitting devices see the light of day? *Chem. Mater.* **26**, 407–414 (2014).
27. Z. W. Seh, J. Kibsgaard, C. F. Dickens, I. Chorkendorff, J. K. Nørskov, T. F. Jaramillo, Combining theory and experiment in electrocatalysis: Insights into materials design. *Science* **355**, eaad4998 (2017).
28. D. L. DuBois, Development of molecular electrocatalysts for energy storage. *Inorg. Chem.* **53**, 3935–3960 (2014).
29. B. D. Steffey, A. Miedaner, M. L. Maciejewski-Farmer, P. R. Bernatis, A. M. Herring, V. S. Allured, V. Carperos, D. L. DuBois, Synthesis and characterization of palladium complexes containing tridentate ligands with PXP (X = C, N, O, S, As) donor sets and their evaluation as electrochemical CO_2 reduction catalysts. *Organometallics* **13**, 4844–4855 (1994).
30. A. D. Wilson, R. H. Newell, M. J. McNevin, J. T. Muckerman, M. Rakowski DuBois, D. L. DuBois, Hydrogen oxidation and production using nickel-based molecular catalysts with positioned proton relays. *J. Am. Chem. Soc.* **128**, 358–366 (2006).
31. J. Y. Yang, R. M. Bullock, W. J. Shaw, B. Twamley, K. Fraze, M. R. DuBois, D. L. DuBois, Mechanistic insights into catalytic H_2 oxidation by Ni complexes containing a diphosphine ligand with a positioned amine base. *J. Am. Chem. Soc.* **131**, 5935–5945 (2009).
32. W. R. McNamara, Z. Han, C.-J. Yin, W. W. Brennessel, P. L. Holland, R. Eisenberg, Cobalt-dithiolene complexes for the photocatalytic and electrocatalytic reduction of protons in aqueous solutions. *Proc. Natl. Acad. Sci. U.S.A.* **109**, 15594–15599 (2012).
33. W. R. McNamara, Z. Han, P. J. Alperin, W. W. Brennessel, P. L. Holland, R. Eisenberg, A cobalt-dithiolene complex for the photocatalytic and electrocatalytic reduction of protons. *J. Am. Chem. Soc.* **133**, 15368–15371 (2011).
34. C. S. Letko, J. A. Panetier, M. Head-Gordon, T. D. Tilley, Mechanism of the electrocatalytic reduction of protons with diaryldithiolene cobalt complexes. *J. Am. Chem. Soc.* **136**, 9364–9376 (2014).
35. V. Bachler, G. Olbrich, F. Neese, K. Wieghardt, Theoretical evidence for the singlet diradical character of square planar nickel complexes containing two *o*-semiquinonato type ligands. *Inorg. Chem.* **41**, 4179–4193 (2002).
36. H. B. Yang, S.-F. Hung, S. Liu, K. Yuan, S. Miao, L. Zhang, X. Huang, H.-Y. Wang, W. Cai, R. Chen, J. Gao, X. Yang, W. Chen, Y. Huang, H. M. Chen, C. M. Li, T. Zhang, B. Liu, Atomically dispersed Ni(I) as the active site for electrochemical CO_2 reduction. *Nat. Energy* **3**, 140–147 (2018).
37. X. Li, W. Bi, M. Chen, Y. Sun, H. Ju, W. Yan, J. Zhu, X. Wu, W. Chu, C. Wu, Y. Xie, Exclusive Ni-N_4 sites realize near-unity CO selectivity for electrochemical CO_2 reduction. *J. Am. Chem. Soc.* **139**, 14889–14892 (2017).
38. X. Zhao, Y. Liu, Unveiling the active structure of single nickel atom catalysis: Critical roles of charge capacity and hydrogen bonding. *J. Am. Chem. Soc.* **142**, 5773–5777 (2020).
39. K. Jiang, S. Siahrostami, A. J. Akey, Y. Li, Z. Lu, J. Lattimer, Y. Hu, C. Stokes, M. Gangishetty, G. Chen, Y. Zhou, W. Hill, W.-B. Cai, D. Bell, K. Chan, J. K. Nørskov, Y. Cui, H. Wang, Transition-metal single atoms in a graphene shell as active centers for highly efficient artificial photosynthesis. *Chem* **3**, 950–960 (2017).
40. A. Le Goff, V. Artero, B. Jousselme, P. D. Tran, N. Guillet, R. Métayé, A. Fihri, S. Palacin, M. Fontecave, From hydrogenases to noble metal-free catalytic nanomaterials for H_2 production and uptake. *Science* **326**, 1384–1387 (2009).
41. T. N. Huan, R. T. Jane, A. Benayad, L. Guetaz, P. D. Tran, V. Artero, Bio-inspired noble metal-free nanomaterials approaching platinum performances for H_2 evolution and uptake. *Energ. Environ. Sci.* **9**, 940–947 (2016).
42. S. Gentil, N. Lalaoui, A. Dutta, Y. Nedellec, S. Cosnier, W. J. Shaw, V. Artero, A. Le Goff, Carbon-nanotube-supported bio-inspired nickel catalyst and its integration in hybrid hydrogen/air fuel cells. *Angew. Chem. Int. Ed.* **56**, 1845–1849 (2017).
43. D. C. Lacy, C. C. L. McCrory, J. C. Peters, Studies of cobalt-mediated electrocatalytic CO_2 reduction using a redox-active ligand. *Inorg. Chem.* **53**, 4980–4988 (2014).
44. R. Cao, R. Thapa, H. Kim, X. Xu, M. Gyu Kim, Q. Li, N. Park, M. Liu, J. Cho, Promotion of oxygen reduction by a bio-inspired tethered iron phthalocyanine carbon nanotube-based catalyst. *Nat. Commun.* **4**, 2076 (2013).
45. Q. Jia, N. Ramaswamy, H. Hafiz, U. Tylus, K. Strickland, G. Wu, B. Barbiellini, A. Bansil, E. F. Holby, P. Zelenay, S. Mukerjee, Experimental observation of redox-induced Fe-N switching behavior as a determinant role for oxygen reduction activity. *ACS Nano* **9**, 12496–12505 (2015).
46. G. Wu, K. L. More, C. M. Johnston, P. Zelenay, High-performance electrocatalysts for oxygen reduction derived from polyaniline, iron, and cobalt. *Science* **332**, 443–447 (2011).
47. J. Han, P. An, S. Liu, X. Zhang, D. Wang, Y. Yuan, J. Guo, X. Qiu, K. Hou, L. Shi, Y. Zhang, S. Zhao, C. Long, Z. Tang, Reordering d orbital energies of single-site catalysts for CO_2 electroreduction. *Angew. Chem. Int. Ed.* **58**, 12711–12716 (2019).
48. W. W. Kramer, C. C. L. McCrory, Polymer coordination promotes selective CO_2 reduction by cobalt phthalocyanine. *Chem. Sci.* **7**, 2506–2515 (2016).
49. Y. Liu, C. C. L. McCrory, Modulating the mechanism of electrocatalytic CO_2 reduction by cobalt phthalocyanine through polymer coordination and encapsulation. *Nat. Commun.* **10**, 1683 (2019).
50. M. Zhu, R. Ye, K. Jin, N. Lazouski, K. Manthiram, Elucidating the reactivity and mechanism of CO_2 electroreduction at highly dispersed cobalt phthalocyanine. *ACS Energy Lett.* **3**, 1381–1386 (2018).
51. T. Abe, T. Yoshida, S. Tokita, F. Taguchi, H. Imaya, M. Kaneko, Factors affecting selective electrocatalytic CO_2 reduction with cobalt phthalocyanine incorporated in a polyvinylpyridine membrane coated on a graphite electrode. *J. Electroanal. Chem.* **412**, 125–132 (1996).
52. J. Wang, X. Huang, S. Xi, H. Xu, X. Wang, Axial modification of cobalt complexes on heterogeneous surface with enhanced electron transfer for carbon dioxide reduction. *Angew. Chem. Int. Ed.* **59**, 19162–19167 (2020).
53. H. Michel, Cytochrome c oxidase: Catalytic cycle and mechanisms of proton pumping-a discussion. *Biochemistry* **38**, 15129–15140 (1999).
54. V. Artero, M. Fontecave, Some general principles for designing electrocatalysts with hydrogenase activity. *Coord. Chem. Rev.* **249**, 1518–1535 (2005).
55. F. A. Armstrong, J. Hirst, Reversibility and efficiency in electrocatalytic energy conversion and lessons from enzymes. *Proc. Natl. Acad. Sci. U.S.A.* **108**, 14049–14054 (2011).
56. X. Zhang, Y.-Y. Li, J. Jiang, R. Zhang, R.-Z. Liao, M. Wang, A dinuclear copper complex featuring a flexible linker as water oxidation catalyst with an activity far superior to its mononuclear counterpart. *Inorg. Chem.* **59**, 5424–5432 (2020).
57. C. Liu, H. Lei, Z. Zhang, F. Chen, R. Cao, Oxygen reduction catalyzed by a water-soluble binuclear copper(II) complex from a neutral aqueous solution. *Chem. Commun.* **53**, 3189–3192 (2017).
58. M. E. Ahmed, S. Chattopadhyay, L. Wang, D. Brazzolotto, D. Pramanik, D. Aldakov, J. Fize, A. Morozan, M. Gennari, C. Duboc, A. Dey, V. Artero, Hydrogen evolution from aqueous solutions mediated by a heterogenized [NiFe]-hydrogenase model: Low pH enables catalysis through an enzyme-relevant mechanism. *Angew. Chem. Int. Ed.* **57**, 16001–16004 (2018).
59. J. Wang, L. Gan, W. Zhang, Y. Peng, H. Yu, Q. Yan, X. Xia, X. Wang, In situ formation of molecular Ni-Fe active sites on heteroatom-doped graphene as a heterogeneous electrocatalyst toward oxygen evolution. *Sci. Adv.* **4**, eaap7970 (2018).
60. L. Bai, C.-S. Hsu, D. T. L. Alexander, H. M. Chen, X. Hu, A cobalt-iron double-atom catalyst for the oxygen evolution reaction. *J. Am. Chem. Soc.* **141**, 14190–14199 (2019).
61. Y. Zhao, K. R. Yang, Z. Wang, X. Yan, S. Cao, Y. Ye, Q. Dong, X. Zhang, J. E. Thorne, L. Jin, K. L. Materna, A. Trimpalis, H. Bai, S. C. Fakra, X. Zhong, P. Wang, X. Pan, J. Guo, M. Flytzani-Stephanopoulos, G. W. Brudvig, V. S. Batista, D. Wang, Stable iridium dinuclear heterogeneous catalysts supported on metal-oxide substrate for solar water oxidation. *Proc. Natl. Acad. Sci. U.S.A.* **115**, 2902–2907 (2018).
62. Y. Zhao, X. Yan, K. R. Yang, S. Cao, Q. Dong, J. E. Thorne, K. L. Materna, S. Zhu, X. Pan, M. Flytzani-Stephanopoulos, G. W. Brudvig, V. S. Batista, D. Wang, End-on bound iridium dinuclear heterogeneous catalysts on WO_3 for solar water oxidation. *ACS Cent. Sci.* **4**, 1166–1172 (2018).
63. S. Zhao, Y. Wang, J. Dong, C.-T. He, H. Yin, P. An, K. Zhao, X. Zhang, C. Gao, L. Zhang, J. Lv, J. Wang, J. Zhang, A. M. Khattak, N. A. Khan, Z. Wei, J. Zhang, S. Liu, H. Zhao, Z. Tang, Ultrathin metal-organic framework nanosheets for electrocatalytic oxygen evolution. *Nat. Energy* **1**, 16184 (2016).

64. S. Zhao, C. Tan, C.-T. He, P. An, F. Xie, S. Jiang, Y. Zhu, K.-H. Wu, B. Zhang, H. Li, J. Zhang, Y. Chen, S. Liu, J. Dong, Z. Tang, Structural transformation of highly active metal-organic framework electrocatalysts during the oxygen evolution reaction. *Nat. Energy* **5**, 881–890 (2020).
65. C. Costentin, S. Drouet, M. Robert, J.-M. Savéant, A local proton source enhances CO_2 electroreduction to CO by a molecular Fe catalyst. *Science* **338**, 90–94 (2012).
66. C. Costentin, J.-M. Savéant, Towards an intelligent design of molecular electrocatalysts. *Nat. Rev. Chem.* **1**, 0087 (2017).
67. C. G. Margarit, C. Schnedermann, N. G. Asimow, D. G. Nocera, Carbon dioxide reduction by iron hangman porphyrins. *Organometallics* **38**, 1219–1223 (2019).
68. E. M. Nichols, J. S. Derrick, S. K. Nistanaki, P. T. Smith, C. J. Chang, Positional effects of second-sphere amide pendants on electrochemical CO_2 reduction catalyzed by iron porphyrins. *Chem. Sci.* **9**, 2952–2960 (2018).
69. A. Chapovetsky, T. H. Do, R. Haiges, M. K. Takase, S. C. Marinescu, Proton-assisted reduction of CO_2 by cobalt aminopyridine macrocycles. *J. Am. Chem. Soc.* **138**, 5765–5768 (2016).
70. C. G. Margarit, N. G. Asimow, M. I. Gonzalez, D. G. Nocera, Double hangman iron porphyrin and the effect of electrostatic nonbonding interactions on carbon dioxide reduction. *J. Phys. Chem. Lett.* **11**, 1890–1895 (2020).
71. D. J. Graham, D. G. Nocera, Electrocatalytic H_2 evolution by proton-gated hangman iron porphyrins. *Organometallics* **33**, 4994–5001 (2014).
72. E. M. Nichols, C. J. Chang, Urea-based multipoint hydrogen-bond donor additive promotes electrochemical CO_2 reduction catalyzed by nickel cyclam. *Organometallics* **38**, 1213–1218 (2019).
73. A. Chapovetsky, M. Welborn, J. M. Luna, R. Haiges, T. F. Miller III, S. C. Marinescu, Pendant hydrogen-bond donors in cobalt catalysts independently enhance CO_2 reduction. *ACS Cent. Sci.* **4**, 397–404 (2018).
74. M. H. Rønne, D. Cho, M. R. Madsen, J. B. Jakobsen, S. Eom, É. Escoudé, H. C. D. Hammershøj, D. U. Nielsen, S. U. Pedersen, M.-H. Baik, T. Skrydstrup, K. Daasbjerg, Ligand-controlled product selectivity in electrochemical carbon dioxide reduction using manganese bipyridine catalysts. *J. Am. Chem. Soc.* **142**, 4265–4275 (2020).
75. M. Rakowski DuBois, D. L. DuBois, The roles of the first and second coordination spheres in the design of molecular catalysts for H_2 production and oxidation. *Chem. Soc. Rev.* **38**, 62–72 (2009).
76. A. Maurin, M. Robert, Noncovalent immobilization of a molecular iron-based electrocatalyst on carbon electrodes for selective, efficient CO_2-to-CO conversion in water. *J. Am. Chem. Soc.* **138**, 2492–2495 (2016).
77. S. Bang, Y.-M. Lee, S. Hong, K.-B. Cho, Y. Nishida, M. S. Seo, R. Sarangi, S. Fukuzumi, W. Nam, Redox-inactive metal ions modulate the reactivity and oxygen release of mononuclear non-haem iron(III)-peroxo complexes. *Nat. Chem.* **6**, 934–940 (2014).
78. S. Fukuzumi, Y. Morimoto, H. Kotani, P. Naumov, Y.-M. Lee, W. Nam, Crystal structure of a metal ion-bound oxoiron(IV) complex and implications for biological electron transfer. *Nat. Chem.* **2**, 756–759 (2010).
79. E. Y. Tsui, R. Tran, J. Yano, T. Agapie, Redox-inactive metals modulate the reduction potential in heterometallic manganese–oxido clusters. *Nat. Chem.* **5**, 293–299 (2013).
80. T. Fukushima, W. Drisdell, J. Yano, Y. Surendranath, Graphite-conjugated pyrazines as molecularly tunable heterogeneous electrocatalysts. *J. Am. Chem. Soc.* **137**, 10926–10929 (2015).
81. X. Zhang, Y. Wang, M. Gu, M. Wang, Z. Zhang, W. Pan, Z. Jiang, H. Zheng, M. Lucero, H. Wang, G. E. Sterbinsky, Q. Ma, Y.-G. Wang, Z. Feng, J. Li, H. Dai, Y. Liang, Molecular engineering of dispersed nickel phthalocyanines on carbon nanotubes for selective CO_2 reduction. *Nat. Energy* **5**, 684–692 (2020).
82. N. Ramaswamy, U. Tylus, Q. Jia, S. Mukerjee, Activity descriptor identification for oxygen reduction on nonprecious electrocatalysts: Linking surface science to coordination chemistry. *J. Am. Chem. Soc.* **135**, 15443–15449 (2013).
83. J. H. Zagal, M. Gulppi, M. Isaacs, G. Cárdenas-Jirón, M. J. S. Aguirre, Linear versus volcano correlations between electrocatalytic activity and redox and electronic properties of metallophthalocyanines. *Electrochim. Acta* **44**, 1349–1357 (1998).
84. J. M. Barlow, J. Y. Yang, Thermodynamic considerations for optimizing selective CO_2 reduction by molecular catalysts. *ACS Cent. Sci.* **5**, 580–588 (2019).
85. X. Zhang, Z. Wu, X. Zhang, L. Li, Y. Li, H. Xu, X. Li, X. Yu, Z. Zhang, Y. Liang, H. Wang, Highly selective and active CO_2 reduction electrocatalysts based on cobalt phthalocyanine/carbon nanotube hybrid structures. *Nat. Commun.* **8**, 14675 (2017).
86. Y. Wu, Z. Jiang, X. Lu, Y. Liang, H. Wang, Domino electroreduction of CO_2 to methanol on a molecular catalyst. *Nature* **575**, 639–642 (2019).
87. G. F. Manbeck, E. Fujita, A review of iron and cobalt porphyrins, phthalocyanines and related complexes for electrochemical and photochemical reduction of carbon dioxide. *J. Porphyrins Phthalocyanines* **19**, 45–64 (2015).
88. J. Pinson, F. Podvorica, Attachment of organic layers to conductive or semiconductive surfaces by reduction of diazonium salts. *Chem. Soc. Rev.* **34**, 429–439 (2005).
89. R. L. McCreery, Advanced carbon electrode materials for molecular electrochemistry. *Chem. Rev.* **108**, 2646–2687 (2008).
90. P. Garrido-Barros, C. Gimbert-Suriñach, D. Moonshiram, A. Picón, P. Monge, V. S. Batista, A. Llobet, Electronic π-delocalization boosts catalytic water oxidation by Cu(II) molecular catalysts heterogenized on graphene sheets. *J. Am. Chem. Soc.* **139**, 12907–12910 (2017).
91. C. J. Kaminsky, J. Wright, Y. Surendranath, Graphite-conjugation enhances porphyrin electrocatalysis. *ACS Catal.* **9**, 3667–3671 (2019).
92. S. Oh, J. R. Gallagher, J. T. Miller, Y. Surendranath, Graphite-conjugated rhenium catalysts for carbon dioxide reduction. *J. Am. Chem. Soc.* **138**, 1820–1823 (2016).
93. M. N. Jackson, C. J. Kaminsky, S. Oh, J. F. Melville, Y. Surendranath, Graphite conjugation eliminates redox intermediates in molecular electrocatalysis. *J. Am. Chem. Soc.* **141**, 14160–14167 (2019).
94. P. D. Tran, A. Le Goff, J. Heidkamp, B. Jousselme, N. Guillet, S. Palacin, H. Dau, M. Fontecave, V. Artero, Noncovalent modification of carbon nanotubes with pyrene-functionalized nickel complexes: Carbon monoxide tolerant catalysts for hydrogen evolution and uptake. *Angew. Chem. Int. Ed.* **50**, 1371–1374 (2011).
95. M. Zhao, Y. Huang, Y. Peng, Z. Huang, Q. Ma, H. Zhang, Two-dimensional metal-organic framework nanosheets: Synthesis and applications. *Chem. Soc. Rev.* **47**, 6267–6295 (2018).
96. S. Lin, C. S. Diercks, Y.-B. Zhang, N. Kornienko, E. M. Nichols, Y. Zhao, A. R. Paris, D. Kim, P. Yang, O. M. Yaghi, C. J. Chang, Covalent organic frameworks comprising cobalt porphyrins for catalytic CO_2 reduction in water. *Science* **349**, 1208–1213 (2015).
97. N. Kornienko, Y. Zhao, C. S. Kley, C. Zhu, D. Kim, S. Lin, C. J. Chang, O. M. Yaghi, P. Yang, Metal-organic frameworks for electrocatalytic reduction of carbon dioxide. *J. Am. Chem. Soc.* **137**, 14129–14135 (2015).
98. A. L. Eckermann, D. J. Feld, J. A. Shaw, T. J. Meade, Electrochemistry of redox-active self-assembled monolayers. *Coord. Chem. Rev.* **254**, 1769–1802 (2010).
99. M. Gilbert Gatty, A. Kahnt, L. J. Esdaile, M. Hutin, H. L. Anderson, B. Albinsson, Hopping versus tunneling mechanism for long-range electron transfer in porphyrin oligomer bridged donor-acceptor systems. *J. Phys. Chem. B* **119**, 7598–7611 (2015).
100. G. S. Mohammad-Pour, K. O. Hatfield, D. C. Fairchild, K. Hernandez-Burgos, J. Rodríguez-López, F. J. Uribe-Romo, A solid-solution approach for redox active metal-organic frameworks with tunable redox conductivity. *J. Am. Chem. Soc.* **141**, 19978–19982 (2019).
101. C. C. L. McCrory, C. Uyeda, J. C. Peters, Electrocatalytic hydrogen evolution in acidic water with molecular cobalt tetraazamacrocycles. *J. Am. Chem. Soc.* **134**, 3164–3170 (2012).
102. N. Kaeffer, A. Morozan, J. Fize, E. Martinez, L. Guetaz, V. Artero, The dark side of molecular catalysis: Diimine-dioxime cobalt complexes are not the actual hydrogen evolution electrocatalyst in acidic aqueous solutions. *ACS Catal.* **6**, 3727–3737 (2016).
103. Z. Weng, Y. Wu, M. Wang, J. Jiang, K. Yang, S. Huo, X.-F. Wang, Q. Ma, G. W. Brudvig, V. S. Batista, Y. Liang, Z. Feng, H. Wang, Active sites of copper-complex catalytic materials for electrochemical carbon dioxide reduction. *Nat. Commun.* **9**, 415 (2018).

Acknowledgments

Funding: This work was funded by the National Research Foundation (NRF), Prime Minister's Office, Singapore, under its Campus for Research Excellence and Technological Enterprise (CREATE) program. We acknowledge financial support from the academic research fund AcRF tier 1 (M4012076 RG118/18), Ministry of Education, Singapore. **Author contributions**: J.W. and X.W. conceived the ideas and wrote the manuscript. S.D. edited the manuscript. X.W. led the writing of the manuscript. **Competing interests**: The authors declare that they have no competing interests. **Data and materials availability**: All data needed to evaluate the conclusions in the paper are present in the paper.

Submitted 23 October 2020
Accepted 5 February 2021
Published 26 March 2021
10.1126/sciadv.abf3989

Citation: J. Wang, S. Dou, X. Wang, Structural tuning of heterogeneous molecular catalysts for electrochemical energy conversion. *Sci. Adv.* **7**, eabf3989 (2021).